DOI: 10.1002/ejic.200700151

Controlled Stabilization and Flocculation of Gold Nanoparticles by Means of 2-Pyrazin-2-ylethanethiol and Pentacyanidoferrate(II) Complexes

Sergio H. Toma,[a] Juliano A. Bonacin,[a] Koiti Araki,[a] and Henrique E. Toma*[a]

Keywords: Aggregation / Colloids / Semi-empirical calculations / Raman spectroscopy / UV/Vis spectroscopy / Charge transfer

2-Pyrazin-2-ylethanethiol (PZT) interacts with gold nanoparticles (AuNps) and pentacyanidoferrates, providing a suitable bridging ligand for the exploitation of the coordination chemistry involved in the stabilization of the colloidal solutions and in the controlled formation of aggregates in the presence of dimethyl sulfoxide. The electronic and vibrational spectra of the molecules have been investigated and discussed based on DFT and ZINDO/S theoretical calculations. The PZT-modified AuNps exhibit strong SERS, coherent with the electromagnetic enhancement mechanism. In contrast, the charge-transfer mechanism seems to predominate in the Raman spectra of the $[Fe(CN)_5PZT]^{3-}$-modified gold nanoparticles.

Introduction

Gold nanoparticles (AuNps) exhibit interesting properties associated with the surface plasmons, allowing a wide range of applications in chemistry, biology, and nanotechnology.[1–4] Most applications require their stabilization as a colloidal solution by means of surface modification with electrically charged species, such as citrate ions, or by using long-chain alkane thiols and detergents.[1–3,5,6] Another method is based on the coordination chemistry analogy between the gold nanoparticles and the transition-metal complexes. According to this approach, the stabilization of the gold nanoparticles can be conveniently performed by means of multifunctional bridging ligands, such as those containing thiol groups, capable of simultaneously binding transition-metal ions and the gold surface atoms.[7] The attractive point of this approach is the possibility of exploiting the controlled charge stabilization promoted by the metal complexes, while incorporating their characteristics and properties into the modified nanoparticles.

Pentacyanidoferrate(II) ions are unique candidates for this purpose, because of their high ionic charges, and suitable kinetic and thermodynamic behavior. Such species have been extensively used to probe the binding affinity of specific donor atoms towards iron ions.[8] This is justified, since the cyanido ligands in the $[Fe(CN)_5]^{3-}$ group are substitution-inert, leaving only one coordinating site for interacting with a specific donor atom of a multifunctional ligand (L).[8,9] On the other hand, the chemical properties of the products, $[Fe(CN)_5L]^{3-}$, are strongly dependent on the nature of L. For instance, pentacyanidoferrate(II) ions show a high affinity for N-heterocycles, amino acids and S-containing ligands, such as sulfoxides, thioethers, and thioamides.[8–16] Interestingly, the affinity of the pentacyanidoferrate(II) ions for thiol groups is relatively small,[7] in contrast to their high affinity for strong π-acceptor ligands, such as pyrazine.[8] Therefore, by using the 2-pyrazin-2-ylethanethiol (PZT) ligand, a preferential binding of the $[Fe(CN)_5]^{3-}$ complex to the pyrazine moiety is expected, leaving the SH group available for interaction with the gold nanoparticles, as illustrated in Figure 1.

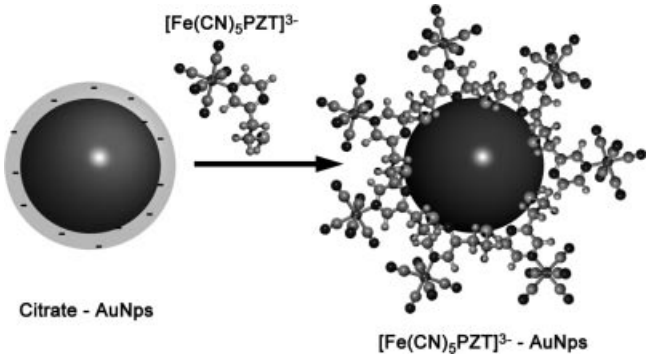

Figure 1. Representation of a gold nanoparticle stabilized with $[Fe(CN)_5PZT]^{3-}$ complexes.

In the presence of dimethyl sulfoxide (dmso) in excess, the pentacyanidoferrate(II) complexes undergo complete ligand exchange, yielding the very stable, colorless $[Fe(CN)_5(dmso)]^{3-}$ complex.[10] In this way, the electrostatic stabilization of the pentacyanidoferrate(II)-modified gold nanoparticles can be removed in the presence of dmso, providing an interesting way of controlling the flocculation of the gold nanoparticles. Because of the many interesting aspects in-

[a] Instituto de Química, Universidade de São Paulo, Caixa Postal 26077, CEP 05513-970 São Paulo, SP, Brazil

volved, we carried out a detailed investigation of this system, focusing especially on the coordination chemistry of pentacyanidoferrates and on the flocculation behavior of the gold nanoparticles, including their characterization based on surface-enhanced Raman scattering (SERS).

Results and Discussion

The electronic configuration of the $[Fe(CN)_5PZT]^{3-}$ complex is typically low-spin, as a consequence of the strong ligand-field strength of the cyanido ligands. The UV/Vis spectrum exhibits two characteristic strong absorption bands at λ_{max} = 266 and 461 nm (log ε = 3.68), ascribed to PZT intraligand π-π* transition, and to metal-to-ligand charge transfer transition, i.e., $d\pi(Fe^{II})\rightarrow p\pi^*(PZT)$, respectively, by analogy with the literature.[8]

The ^1H NMR spectrum of the pentacyanidoferrate(II) complex in ^2H_2O exhibits the characteristic downfield shift of the signals of the adjacent aromatic protons (*α*) of the N-heterocycles coordinated to the $Fe(CN)_5^{3-}$ moiety, changing from δ = 8.41 to 9.03 ppm for $H^{2'}$ and from δ = 8.41 to 8.93 ppm for the H^2 signal in respect of the free ligand. This behavior follows the spectroscopic trends for monomeric pentacyanidoferrate(II) complexes, as shown in Figure 2, in which the downfield shift increases from 4-methylpyridine ($\Delta\delta^1H$ = 0.40 ppm) ≈ pyridine ($\Delta\delta^1H$ = 0.33 ppm) < isonicotinamide ($\Delta\delta^1H$ = 0.40 ppm) < pyrazine ($\Delta\delta^1H$ = 0.50 ppm) < *N*-methylpyrazinium ion ($\Delta\delta^1H$ = 0.80 ppm). For the PZT α-proton signals, downfield shifts of $\Delta\delta^1H^{2'}$ = 0.62 ppm and $\Delta\delta^1H^2$ = 0.52 ppm were observed, which are close to that expected from the spectrochemical series (E_{TE} = 21.7 kK). The PZT β-aromatic proton signal underwent an upfield shift from δ = 8.34 to 8.14 ppm.

The observed behavior of the aromatic protons in pentacyanidoferrate(II) N-heterocyclic complexes involves main contributions from the $d\pi\rightarrow p\pi$ back-bonding to the heterocyclic ligand and the opposing inductive effect, whereas for the α-protons the magnetic anisotropy due to the electron looping at the CN axis bond is most relevant.[17] Curiously, the thiol proton signal exhibits a pronounced change in the chemical shift with respect to that of the free PZT ligand, i.e., from δ = 1.43 (^2H_2O) or 1.46 (C^2HCl_3) to 3.33 ppm in the pentacyanidoferrate(II) complex. This effect can be ascribed to the magnetic anisotropy of the cyanido ligands, producing a deshielding effect on the nuclei located perpendicular to this triple bond. As the thiol proton lies in a deshielding region, a large downfield shift is observed. Another evidence of the magnetic anisotropy of the cyanido ligands is reflected in the shape of the thiol proton peak. In fact, in ^2H_2O, the S–H signal of the free PZT ligand appears as a broad coalescent peak at δ = 1.43 ppm. After coordination to the pentacyanidoferrate(II) complex, this peak became rather narrow, at δ = 3.33 ppm, exhibiting a strong spin-decoupling effect, removing the triplet feature observed in aprotic solvents.

Cyclic voltammetry (CV) and differential pulse voltammetry (DPV) for $[Fe(CN)_5PZT]^{3-}$ exhibited only a single redox process at 0.55 V (SHE), $E_{pa} - E_{pc}$ = 60 mV, showing no evidence of formation of dinuclear or any other species in solution. The $E_{1/2}$ is in good agreement with the analogous $[Fe(CN)_5pz]^{3-}$ (pz = pyrazine) species (0.55 V vs. SCE).[8]

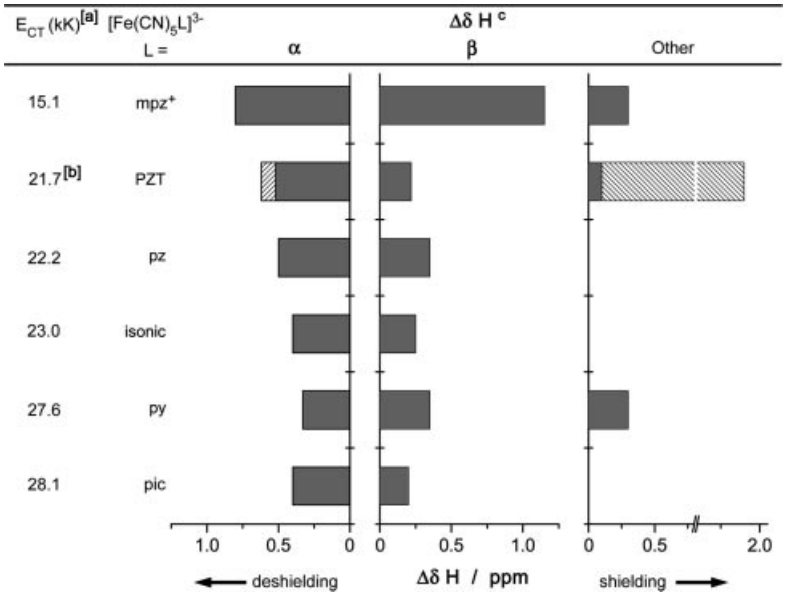

Figure 2. $\Delta\delta(^1H)$ for the protons α, β and others in pentacyanidoferrate(II) complexes of aromatic N-heterocycles, L. [a] Energy of metal-to-ligand charge transfer from ref.[17] and this work. [b] $\Delta\delta(^1H)$ for the α, β and other protons in ^2H_2O. Striped bars correspond to $H^{2'}$ (*α*) and S–H signals (other). mpz^+ = *N*-methylpyrazinium ligand; PZT = 2-pyrazin-2-ylethanethiol; pz = pyrazine; isonic = isonicotinamide; py = pyridine; pic = 4-methylpyridine.

Solvatochromic Behavior

Cyanidoiron complexes exhibit strong solvent effects influencing their chemical reactivity and solvatochromic behavior.[18–22] Such solvent effects arise from specific donor–acceptor interactions of the solvent molecules with the available nonbonding electron pairs of the cyanido ligands. For this reason, the observed solvatochromism is best correlated with the acceptor number[23] (AN) of the solvents. In Figure 3 the normalized spectra of $[Fe(CN)_5PZT]^{3-}$ in the different solvents are shown.

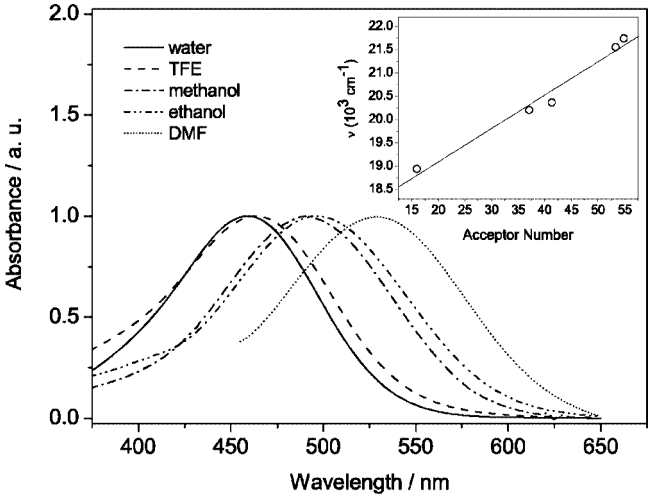

Figure 3. Normalized spectra of the $[Fe(CN)_5PZT]^{3-}$ complex in several solvents, as a function of the acceptor number: (——) water (AN = 54.8), (– – –) trifluoroethanol (TFE) (AN = 53.3), (– · – · –) methanol (AN = 41.3), (– ·· – ·· –) ethanol (AN = 37.1), (···) DMF (AN = 16.0). Inset: Correlation between the MLCT band energies of the $[Fe(CN)_5PZT]^{3-}$ complex and the AN parameter of the solvents (water, trifluoroethanol, methanol, ethanol, DMF).

As expected, the energy of the charge-transfer band shows a strong dependence with the solvent acceptor number.[20–22] Solvents displaying high AN values are able to interact with the nitrogen electron pair on the cyanido ligands, removing part of σ-electron density, while increasing the dπ→pπ* back-bonding contribution. This leads to the stabilization of the occupied metal dπ orbitals, thus increasing the energies of the MLCT bands, as expressed by the equation:[20]

$$\nu_s = \nu_0 + a(AN)$$

where ν_s is the experimental wavenumber and ν_0 corresponds to the extrapolated value at AN = 0 (Figure 3, inset). The parameter a measures the sensitivity of the charge-transfer band to the solvent acceptor properties. For the $[Fe(CN)_5PZT]^{3-}$ complex, ν_0 = 17660 cm^{-1}, and a = 72 cm^{-1}.

Theoretical Simulation of the Electronic Spectrum

The DFT-optimized geometry for the $[Fe(CN)_5PZT]^{3-}$ ion is consistent with an octahedral configuration, with four equatorial Fe–C and C≡N bonds of 1.982 and 1.178 Å, respectively. The corresponding axial bond lengths were 1.970 and 1.176 Å, respectively, reflecting the *trans*-influence of the dπ→pπ* interactions from the Fe–PZT moiety. On the basis of the DFT-optimized geometry, ZINDO/S calculations were carried out, simulating the electronic spectrum of the $[Fe(CN)_5PZT]^{3-}$ ion, with the MLCT band at 17827 cm^{-1} displaying an oscillator strength of 0.496. This theoretical value refers to a vacuum calculation, and differs significantly from the experimental value of 21700 cm^{-1} in aqueous solution, coinciding, however, with the extrapolated value at AN = 0 (ν_0 = 17660 cm^{-1}).[20] This observation is quite relevant, justifying a careful investigation of the solvatochromic effects, prior to the theoretical simulation of the electronic spectra.

According to the theoretical calculations, the observed MLCT transition involves the HOMO→LUMO (MOs 52→53) excitation. The composition of the HOMO and LUMO levels is shown in Table 1. The HOMO level (MO-52) is mainly composed of the metal dπ orbitals (68%), as illustrated in Figure 4, while the LUMO (MO-53) has the largest contribution from the PZT π* orbitals (Figure 4, B).

Table 1. MOs' percent composition obtained from ZINDO/S calculations.

	HOMO	LUMO
MO	52	53
Energy [eV]	1.8834	7.1168
% Fe	68.36[a]	13.45[b]
% CN	14.56	28.55
% PZT	17.08	58.00

[a] d(xz): 39.25%, d(yz): 29.06%, d(xy): 0.02%, d(z^2): 0.02%, d(x^2–y^2): 0.01%. [b] d(xz): 7.64%, d(yz): 5.80%, d(xy): 0.01%, d(z^2): 0.00%, d(x^2–y^2): 0.00%.

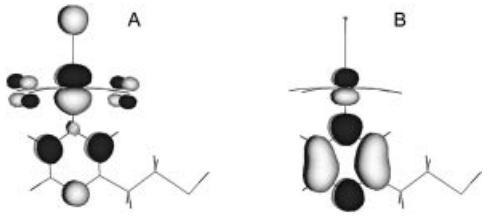

Figure 4. Plots of the frontier orbitals of the $[Fe(CN)_5PZT]^{3-}$ (A) HOMO and (B) LUMO.

Vibrational Study of PZT and $[Fe(CN)_5PZT]^{3-}$

In Figure 5 is shown the FT-IR spectra of the PZT ligand and its corresponding pentacyanidoferrate(II) complex. The IR spectrum of PZT exhibits the characteristic high-energy frequencies associated with the C–H stretching modes of the $–CH_2–CH_2–$ group, and a broad band at 2540 cm^{-1} related to the S–H stretching vibration. In the pentacyanidoferrate(II) complex, the FT-IR spectrum presents two characteristic bands at ca. 2050 and 570 cm^{-1} associated with the vibrational modes of the C≡N and Fe–CN bonds. The S–H stretching mode can also be detected in the FTIR spectra, shifting from 2540 to 2470 cm^{-1} upon the N-coordination to the pentacyanidoferrate complex,

corroborating the observed influence on the S–H group in the NMR spectrum.

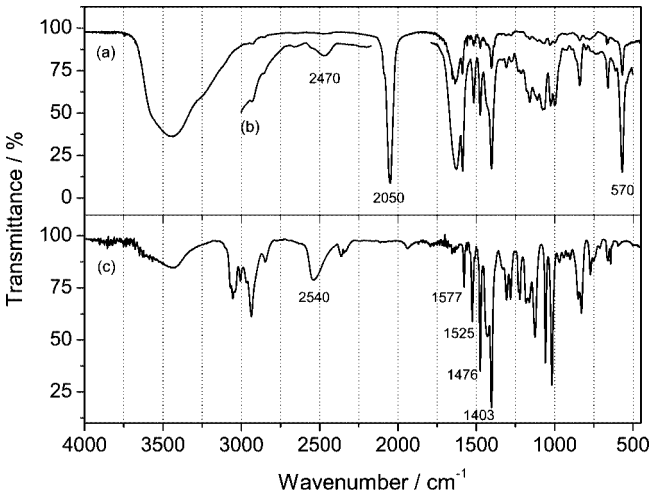

Figure 5. IR spectra of $Na_3[Fe(CN)_5PZT]\cdot 3H_2O$ in KBr pellets: (a) diluted and (b) three times more concentrated, (c) IR spectrum of pure liquid PZT.

The Raman spectrum of the PZT ligand is dominated by two intense bands at 1058 and 1018 cm^{-1} ascribed to the vibrational modes of the $–CH_2–CH_2–$ and pyrazine moieties, respectively.

The complete assignment of the PZT and $Na_3[Fe(CN)_5$-PZT]$\cdot 3H_2O$ vibrational frequencies was carried out based on the theoretical calculations, as shown in Tables 2 and 3.

Interaction of Gold Nanoparticles with PZT

The colloidal solutions of citrate-stabilized gold nanoparticles (average size 20 nm) exhibit a characteristic red-wine color ascribed to the optical interaction with the surface plasmons, as accounted for by the Mie theory.[24] The spectral variation of the gold nanoparticles in the presence of PZT (1×10^{-5} mol dm^{-3}) can be seen in Figure 6. After the addition of PZT to the gold nanoparticles solution, the intensity of the plasmon absorption band at 520 nm decreases in parallel with the rise of a new band above 600 nm. As this band becomes more intense, there is a bathochromic shift to 660 nm. Such optical changes can be

Table 2. Assignment of calculated wavenumber [cm^{-1}] to experimental bands in the FT-IR and Raman of PZT.

Mode	Experimental		Calculated	Assignment
	FT-IR	Raman	frequencies	
45	3069 (w)	–	3175	ν C–H_{pz}
44	3054 (w)	–	3170	ν C–H_{pz}
43	3007 (m)	–	3143	ν C–H_{pz}
42	2968 (w)	–	3098	ν_{as} C–H^2
41	2937 (m)	–	3051	ν_s C–H^2; ν_{as} C–H^2
40		–	3042	ν_{as} C–H^2; ν_s C–H^2
39	2847 (w)	–	3020	ν_s C–H^2; ν_{as} C–H^2
38	2540 (w)	–	2678	ν S–H
37	1577 (m)	1577 (m)	1609	ν ring; δ C–H^2
36			1581	ν ring; ω C–H^2
35	1525 (m)	1525 (w)	1511	δ C–H_2
34	1475 (s)	–	1504	δ C–H_{pz}; ν C–$C_{pz–eth}$
33	1428 (s)	1428 (w)	1490	δ C–H^2
32	1403 (vs)	1403 (sh)	1425	δ C–H_{pz}; ω C–H_2; ν C–N_{pz}
31	1331 (w)	1331 (vw)	1370	ω C–H^2; δ C–H_{pz}
30	1307 (m)	1307 (vw)	1315	δ C–H_{pz}; ω C–H^2
29	1282 (m)	1275 (vw)	1288	τ C–H^2
28		1248 (vw)	1265	ω C–H^2; δ C–H_{pz}; ν C–$C_{pz–eth}$
27	1231 (m)	1231 (vw)	1251	ω C–H^2; δ C–H_{pz}
26	1223 (m)		1205	ω C–H^2; δ S–H
25	1183 (m)	1183 (vw)	1188	δ C–H_{pz}; ω C–H^2; δ S–H
24	1163 (m)	1163 (vw)	1150	τ C–H^2
23	1125 (s)	1058 (s)	1091	ν C–C_{eth}; δ C–H_{pz}; δ S–H
22	1058 (s)		1070	
21	1018 (s)	1018 (s)	1029	ν ring
20	969 (vw)	969 (vw)	996	π ring; τ C–H_2; ρ C–H^2
19	940 (vw)	–	982	τ C–H^2; π ring; ρ C–H^2
18	920 (vw)	–	944	π ring; τ C–H_2; ρ C–H^2
17	840 (m)	873 (w)	908	δ S–H; ω C–H^2; ν ring
16	830 (m)	830 (m)	848	π ring; ρ C–H^2
15			830	δ ring; ν C–C_{eth}; δ S–H
14	771 (w)	774 (w)	780	π ring; ρ C–H_2; τ C–H^2
13	750 (w)	738 (m)	760	ν S–C; δ ring
12	661 (w)	660 (m)	690	ρ C–H_2; π ring
11	643 (w)	632 (m)	650	δ ring; ν C–$C_{pz–eth}$; ν S–C
10	–	589 (vw)	588	δ ring; ν C–$C_{pz–eth}$; ν S–C
9	–	500 (w)	465	π ring; τ C–H^2; ρ C–H^2

Table 3. Assignment of calculated wavenumber [cm^{-1}] to experimental bands in the FT-IR and Raman of $Na_3[Fe(CN)_5PZT]$.

Mode	Experiment		Calculated	Assignment
	FT-IR	Raman	frequencies	
71	2470 (m)	–	2649	ν S–H
70		–	2189	ν C≡N
69		–	2181	ν C≡N
68	2050 (vs)	–	2176	ν C≡N
67		–	2169	ν C≡N
66		–	2167	ν C≡N
65	1590 (s)	1590 (s)	1620	ν ring; δ $C–H^2_{eth}$
64	1516 (m)	–	1505	δ $C–H^2_{eth}$
63	1476 (m)	–	1497	δ $C–H_{pz}$; δ $C–H^2_{eth}$
62		–	1492	δ $C–H^2_{eth}$; δ $C–H_{pz}$
61	1430 (sh)	–	1481	δ $C–H^2_{eth}$; δ $C–H_{pz}$
60	1403 (s)	–	1439	δ $C–H_{pz}$; ω CH_{2eth}; ν $C–N_{pz}$
59		–	1373	ω $C–H^2_{eth}$; δ $C–H_{pz}$
58	1308 (vw)	1308 (vw)	1320	ω $C–H^2_{eth}$; τ $C–H^2_{eth}$; δ $C–H_{pz}$
57			1312	τ $C–H^2_{eth}$; τ $C–H^2_{eth}$; δ $C–H_{pz}$
56	1277 (vw)	–	1290	ω $C–H^2_{eth}$; δ $C–H_{pz}$
55	1233 (vw)	1241 (vw)	1268	δ $C–H_{pz}$; ω $C–H^2_{eth}$
54	1214 (vw)	–	1225	ω $C–H^2_{eth}$; δ $C–H_{pz}$
53	1179 (sh)	1179 (sh)	1177	τ $C–H^2_{eth}$; δ $C–H_{pz}$
52	1159 (m)	1159 (m)	1159	δ $C–H_{pz}$; τ $C–H^2_{eth}$;
51	1110 (m)	1076 (m)	1081	ν $C–C_{pz–eth}$; δ $C–H_{pz}$; δ S–H
50	1076 (m)		1079	δ$C–H_{pz}$; ν $C–C_{pz–eth}$; δ S–H
49	1026 (w)	1034 (m)	1033	τ $C–H^2_{eth}$; ring breathing
48	998 (w)	–	1030	ring breathing; τ $C–H^2_{eth}$
47	970 (sh)	–	936	π ring; τ $C–H^2_{eth}$
46			916	ν $C–C_{eth}$; δ S–H; ring breathing
45	867 (sh)	867 (vw)	869	π ring; ρ $C–H^2_{eth}$
44	841 (w)	841 (w)	850	δ ring; δ S–H; ν $C–C_{eth}$
43	800 (vw)	800 (vw)	832	π ring (54.9) + ρ C^8H_2 (28.0) + ρ $C^7–H^2$ (14.2)
42			807	ρ $C–H^2_{eth}$; π ring
41	659 (w)	659 (s)	724	π ring; ν S–C; ρ $C–H^2_{eth}$
40			720	π ring; ν S–C; ρ $C–H^2_{eth}$
39			678	δ ring; ν S–C
38	612 (vw)	612 (w)	591	δ ring; ω $C–H^2_{eth}$; ν S–C
37			577	π ring; ρ $C–H^2_{eth}$; π Fe–C (17.4)
36			534	π Fe–C; π ring
35	570 (s)	570 (s)	526	π Fe–C; π ring; δ S–C
34			505	π Fe–C; π ring; ρ $C–H^2_{eth}$
33			463	π Fe–C; π ring
32		500 (w)	460	π Fe–C; π ring; ρ $C–H^2_{eth}$

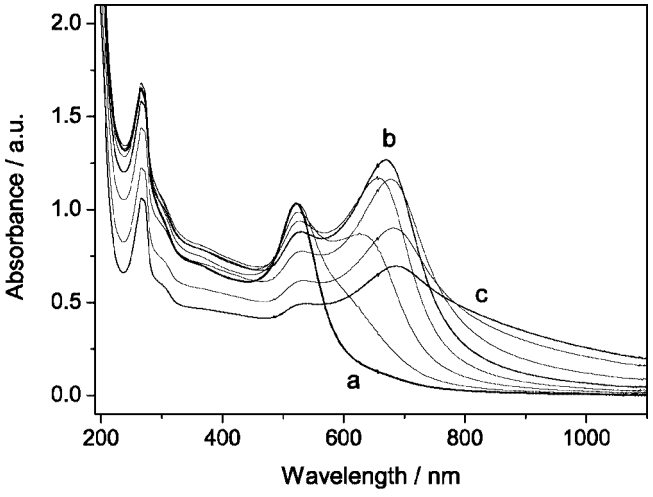

Figure 6. Changes of the UV/Vis spectra of AuNps upon addition of the PZT (1×10^{-5} mol dm^{-3}) ligand as a function of time: (a) starting solution (t = 0 min), (b) flocculation (t = 42 min), (c) precipitation (t = 90 min).

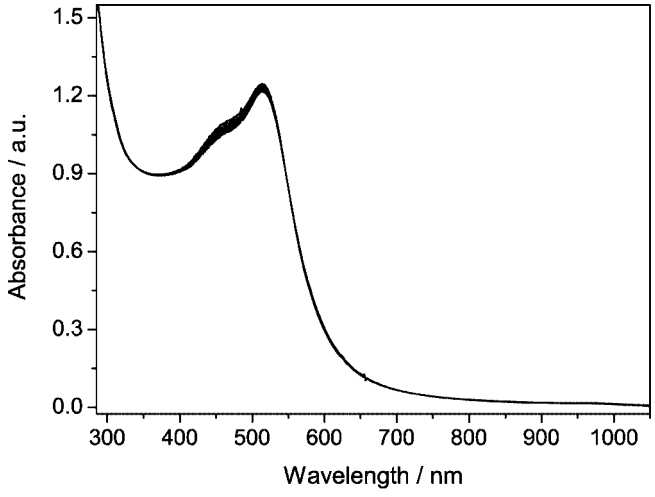

Figure 7. Successive UV/Vis spectra of AuNps showing only a very small decrease of intensity, after adding 1×10^{-5} mol dm^{-3} $[Fe(CN)_5PZT]^{3-}$ (t = 120 min).

ascribed to the aggregation of the gold nanoparticles, arising from the mutual interference of the plasmon levels in neighboring nanoparticles.[1] The intensity of the 660 nm band reaches a maximum, after which there is a gradual decay and shift to about 700 nm, due to the precipitation process.

A contrasting behavior is observed for the $[Fe(CN)_5PZT]^{3-}$-modified AuNps. In Figure 7 the spectra of the AuNps upon addition of $[Fe(CN)_5PZT]^{3-}$ (1×10^{-5} mol dm^{-3}) is shown. The characteristic MLCT band at 460 nm for the $[Fe(CN)_5PZT]^{3-}$ complex can be observed as a shoulder of the plasmon resonance band at 520 nm, exhibiting only a small decrease in intensity after the binding and replacement of the citrate shell of the gold nanoparticles. In this case, a stable colloidal solution is obtained, which can be stored for many days, under argon, without any evidence of the plasmon coupling band above 600 nm, associated with flocculation.

SERS Effect on PZT-AuNps and $Na_3[Fe(CN)_5PZT]$-AuNps

Because of the expected occurrence of SERS, the aggregated PZT-AuNps in aqueous media were also studied by Raman spectroscopy. Typical spectra can be seen in Figure 8, in comparison with the normal Raman spectra of the PZT ligand (pure form).

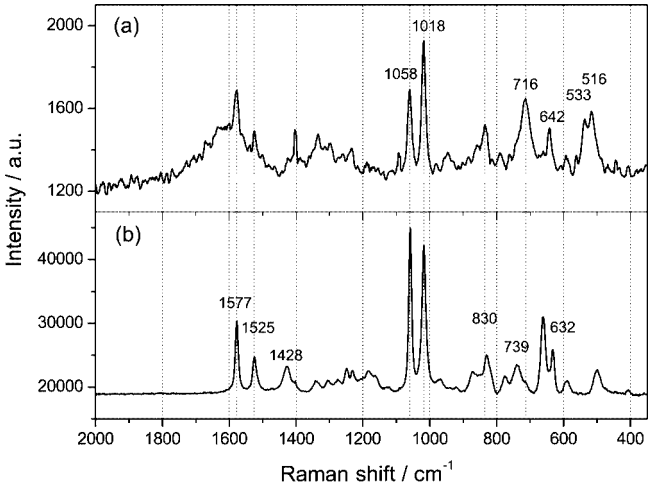

Figure 8. SERS spectrum of the PZT-AuNps ([PZT] = 1×10^{-5} mol dm^{-3}) (a) and Raman spectrum of the PZT in pure liquid form (b).

Considering the very low concentrations ([PZT] = 10^{-5} mol dm^{-3}) employed in the measurements, the strong (SERS) intensification of the PZT vibrational peaks becomes quite evident in Figure 8. It is known that the SERS effect can involve either electromagnetic (EM)[25] or charge transfer (CT)[26] mechanisms. In the EM model, the Raman enhancement is attributed to the excitation of the surface plasmon polaritons by the exciting wavelength, as described by the Mie formalism.[24] This mechanism is typically observed in the case of plasmon resonance involving physically adsorbed molecules.[27] Usually, SERS of particles smaller than the exciting wavelength are a function of the radius and refractive index, and the maximum enhancement is observed when the molecules are as close as possible to the surface and the incident and scattered waves are perpendicular to the scattering plane.

In the case of chemically adsorbed molecules, a charge-transfer mechanism becomes plausible. Generally, it involves the transfer of an electron from the Fermi level of the metal atom to an unoccupied molecular orbital of the adsorbate or vice versa, but the evidence of this particular type of excitation has been mainly obtained from electrochemical experiments. It should be noted that SERS can be observed even for chemically adsorbed molecules without charge-transfer resonance.[27] When charge-transfer resonance and surface-enhanced resonance Raman scattering are involved, the mechanism is referred to as SERRS (Surface Enhanced Resonance Raman Scattering). One of the first reports on the SERRS mechanism dealt with the $[\{Fe(CN)_5\}_2(\mu\text{-bipy})]^{6-}$ complex adsorbed on a silver electrode.[28] Although a direct spectroscopic evidence has not been obtained in this case, it is important to notice that outer-sphere charge-transfer excitation in pentacyanidoferrate(II) complexes have already been reported in the literature,[29,30] as well as in TiO_2 films containing anchored $[Fe(CN)_5L]^{n-}$ species.[31]

In the case of the PZT-AuNps, the aggregation phenomenon in aqueous solution leads to the selective enhancement of the vibrational modes associated with the PZT ligand, involving both the pyrazine ring and thioalkane moieties. It is interesting to note that the relative intensity of the peaks at 1058 and 1018 cm^{-1} associated with ethanethiol and pyrazine vibrational modes, respectively, is inverted in relation to the normal Raman spectrum of the PZT species. The peaks at ca. 738 and 500 cm^{-1}, ascribed to C–S stretching and–CH_2–CH_2– vibrational modes undergo strong enhancement, shifting to 716 and 516 cm^{-1}, respectively. This is in agreement with the electromagnetic mechanism, since such groups are in close proximity to the gold surface due to the thiol binding.

The Raman spectrum of the pentacyanidoiron-stabilized AuNps shows a strong enhancement of the vibrational modes, exhibiting a rather contrasting profile in relation to the normal spectrum of the isolated complex, as can be observed in Figure 9.

The 659 cm^{-1} peak ascribed to the C–S stretching mode exhibits the greatest enhancement, shifting to 700 cm^{-1}. The original peaks at 1590, 1159, 1076, and 1034 cm^{-1} in the normal spectra practically vanish and some new peaks arise in this region. This result suggests a different origin for the SERS effect in the $[Fe(CN)_5PZT]^{3-}$-stabilized AuNps, in comparison with the PZT-AuNps aggregates. The enhancement of the new bands seems to be associated with the electronic character of the excited state, and the occurrence of a charge-transfer mechanism can be plausible in this case. The puzzling point, however, is that there is no plasmon coupling band above 600 nm, as in the case of the PZT-AuNps. Presumably, an interfacial charge-transfer excitation is involved, as in the preceding example involving

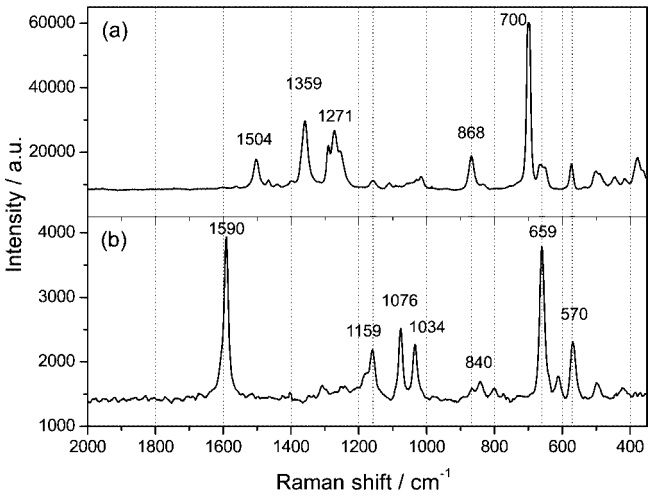

Figure 9. SERS spectrum of the complex $Na_3[Fe(CN)_5PZT]$ at 10^{-5} mol dm^{-3} stabilizing AuNps (a) and Raman spectrum of the iron complex at 1 mol dm^{-3} in aqueous solution (b).

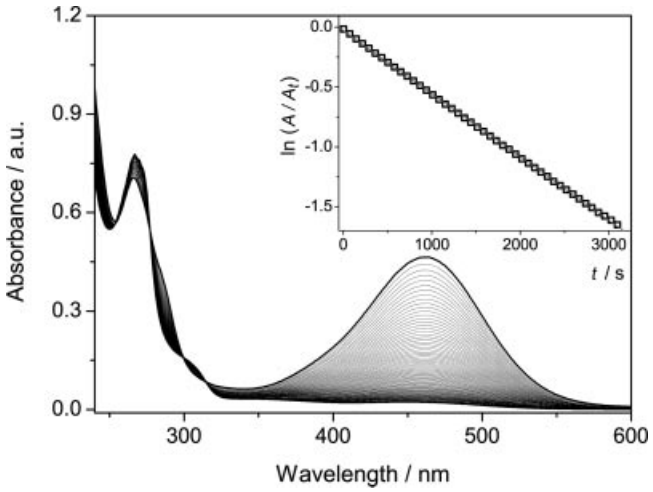

Figure 10. UV/Vis spectra of 1×10^{-4} mol dm^{-3} $[Fe(CN)_5PZT]^{3-}$ in the presence of 0.5 mol dm^{-3} dmso. Inset: first-order kinetic plot, where $k_{obs} = 5.2 \times 10^{-4}$ s^{-1} with 99.9% correlation.

cyanidoiron complexes, from the literature.[28] In addition, it has been shown that many chromophore-functionalized gold nanoparticles[32] undergo complete quenching of emission, from such interfacial charge transfer effects. At the present time, the SERS phenomenon and their many variations are not yet completely understood,[27] and the unusual behavior of the $[Fe(CN)_5PZT]^{3-}$-stabilized AuNps will be subject of a future, detailed investigation.

Dissociation Kinetics of $[Fe(CN)_5PZT]^{3-}$ and Controlled Aggregation of the Modified Gold Nanoparticles

The dissociation kinetics of the $[Fe(CN)_5PZT]^{3-}$ complex was studied in the presence of a large excess of dimethyl sulfoxide as the attacking ligand. The resulting $[Fe(CN)_5dmso]^{3-}$ complex is quite stable, and does not absorb in the visible region.[10] Therefore, the dissociation reaction can be conveniently monitored by the disappearance of the MLCT band at 461 nm.

The substitution kinetics of the PZT ligand by dmso, in large excess (0.5 mol dm^{-3}), proceeded according to first-order kinetics, as shown in Figure 10 (inset). It should be noted that ligand substitution in aromatic N-heterocycle pentacyanidoferrates(II) complexes occurs by a dissociative mechanism,[8–13] as expressed by the equations:

$$[Fe(CN)_5pzt]^{3-} \underset{k_{-PZT}}{\overset{k_{PZT}}{\rightleftharpoons}} [Fe(CN)_5]^{3-} + pzt$$

$$[Fe(CN)_5]^{3-} + H_2O \underset{k_1}{\overset{k_{-1}}{\rightleftharpoons}} [Fe(CN)_5H_2O]^{3-}$$

$$[Fe(CN)_5]^{3-} + dmso \xrightarrow{k_{dmso}} [Fe(CN)_5dmso]^{3-}$$

$$k_{obs} = \frac{k_{-PZT}\, k_{dmso}\, [dmso]}{k_{PZT}\, [PZT] + k_{dmso}[dmso]}$$

As previously shown,[8] under pseudo-first-order conditions, and assuming steady-state hypothesis for the $[Fe(CN)_5]^{3-}$ intermediate, the observed rate constants are given by:

In the presence of a large excess of dmso, $k_{dmso}[dmso] >> k_{PZT}[PZT]$, and the observed rate constant coincides with the limiting dissociation rate constant for the $[Fe(CN)_5PZT]^{3-}$ complex, i.e., $k_{obs} = k_{-PZT}$.

The same pattern was also observed (Figure 11) for the $[Fe(CN)_5PZT]^{3-}$-stabilized gold nanoparticles in the presence of dmso (0.5 mol dm^{-3}). As observed for the free complex, the reaction with dmso leads to an exponential decrease of the MLCT band at ca. 460 nm (Figure 11, inset), with a kinetic dissociation constant of 6.2×10^{-4} s^{-1}. This value is comparable to 5.2×10^{-4} s^{-1} obtained for the free complex.

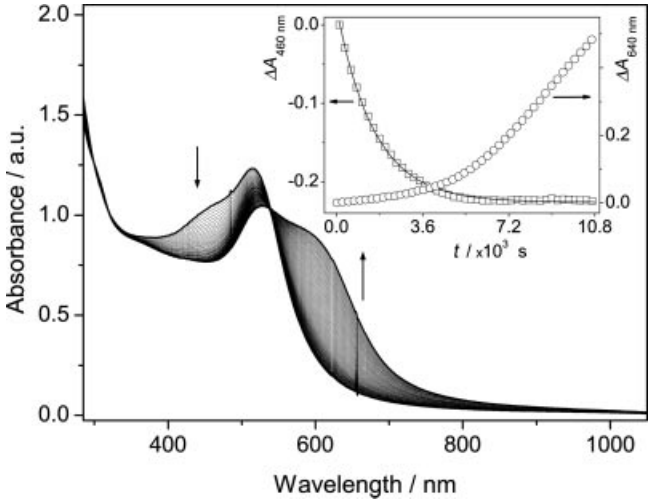

Figure 11. UV/Vis spectra and dissociation kinetics of the $[Fe(CN)_5PZT]^{3-}$-stabilized gold nanoparticles after addition of 0.5 mol dm^{-3} dmso. Inset: Decrease of absorbance at 460 (□, left) and 640 nm (○, right). The solid line is a pseudo-first-order behavior fit at 460 nm, where $k_{obs} = 6.2 \times 10^{-4}$ s^{-1} with 99.8% of correlation.

It should be noted that the dissociation of the pentacyanidoferrate(II) complex from the AuNps surface removes the electrostatic stabilization of the nanoparticles. Therefore, as

Table 4. Kinetic and thermodynamic data for $[Fe(CN)_5L]^{2-/3-}$ complexes.[a]

Ligand	E_{CT} 10^3 cm^{-1}	Donor group	k_d^{II} $\times10^{-4}$ s^{-1}	k_f^{II} $\times10^{2}$ mol^{-1} s^{-1}	K_f^{II} $\times10^{5}$ dm^3 mol^{-1}	K_f^{III} dm^3 mol^{-1}	$E°_L$[b]	Ref.
dmso	–	S=O	0.75	2.4	49	3.7×10^{-2}	850	[10–12]
Methylpyrazinium	15.1	C=N	2.8	5.5	20	4.7×10^{-1}	780	[10,33]
Pyrazine	22.2	C=N	4.2	3.80	9.0	1.7×10^{3}	550	[8,11,12,15,16]
PZT	21.7	C=N	5.2	3.8[c]	7.3[c]	1.4×10^{3}[c]	550	–
AuNps-PZT	21.7	C=N	6.4	–	–	–	–	–
Isonicotinamide	23.0	C=N	7.3	2.95	8.2	5.2 x10^3	500	[8,11,12,15,16]
4-Mercaptopyridine	24.7	C=N	11.0	2.9	2.6	3.4×10^{4}	442	[7]
Pyridine	27.6	C=N	11.0	3.65	4.6	9.4×10^{3}	470	[8,11,12,15,16]

[a] The complexes are listed in decreasing order of reduction potential. [b] In mV (SHE). [c] Estimated values based on assumed value of the pyrazine: k_f^{II} = 380 mol^{-1} s^{-1}.

expected, the ligand-substitution reaction is followed by the flocculation of the resulting PZT-AuNps, leading to an increase of the absorbance at 640 nm, i.e.:

$[Fe(CN)_5PZT]$-AuNps + dmso → $[Fe(CN)_5dmso]^{3-}$ + PZT-AuNps

PZT-AuNps → flocculation

From the kinetics and electrochemical parameters obtained in this work, it is possible to estimate the equilibrium constants for $[Fe(CN)_5PZT]^{3-}$ and to compare with related systems, as shown in Table 4. The results are rather consistent, indicating that the characteristic properties of the pentacyanidoferrate(II) complexes are preserved after their binding to the gold nanoparticles.

Conclusions

Gold nanoparticles and pentacyanidoferrates can be successfully combined by means of a suitable bridging ligand such as 2-pyrazin-2-ylethanethiol, allowing the exploitation of the coordination chemistry involved, especially, the stabilization of the colloidal solutions and the controlled formation of aggregates in the presence of a strong ligand, such as dimethyl sulfoxide. The modified gold nanoparticles exhibit a strong SERS effect. The results are coherent with the enhancement by the electromagnetic mechanism for the PZT-modified gold nanoparticles, while the charge-transfer mechanism seems to predominate in the case of the $[Fe(CN)_5PZT]^{3-}$-modified gold nanoparticles. The reported strategy, based on a typical coordination chemistry approach, can be extended to the generation of functional, self-assembled nanoparticle films, of great relevance in molecular devices.

Experimental Section

Materials: All solvents and reactants used in this work were of analytical grade and used as supplied. $HAuCl_4{\cdot}3H_2O$, trisodium citrate hydrate, and 2-pyrazin-2-ylethanethiol (PZT), were purchased from Aldrich. $Na_3[Fe(CN)_5NH_3]{\cdot}3H_2O$ was prepared from sodium nitroprusside, $Na_3[Fe(CN)_5NO]{\cdot}2H_2O$ (Carlos Erba), according to the usual procedure.[34] All aqueous solutions were prepared using MilliQ water (18.2 MΩ cm). Citrate-stabilized gold nanoparticles (AuNps) were prepared according to the Turkevitch[35] method as described previously.[7] The concentration of gold nanoparticles suspension used in the experiments was calculated as 10^{-9} mol dm^{-3}, assuming a total conversion of $AuCl_4^-$ ions into colloidal nanoparticles of 20 nm average size, as previously measured by MEV and STM on HOPG substrate. The calculated area per particle was 1.26×10^{-15} m^2, yielding a total surface area of 0.756 m^2 dm^{-3}. $Na_3[Fe(CN)_5PZT]{\cdot}3H_2O$ was prepared by adapting the procedures described by Toma et al.[8–14] $Na_3[Fe(CN)_5NH_3]{\cdot}3H_2O$ (0.326 g or 1.0 mmol) was mixed with a tenfold excess of 2-pyrazin-2-ylethanethiol (1.40 g or 10.0 mmol) in 10 mL of water, and the mixture magnetically stirred at room temperature under argon for 30 min. The product precipitated by addition of ethanol, and was collected on a glass filter, washed with cold ethanol and dried under vacuum. Yield: 84%. $Na_3[Fe(CN)_5PZT]{\cdot}3H_2O$: $C_{11}H_{14}FeN_7Na_3SO_3$ (449.15): calcd. C 30.4, H 3.24, N 19.3; found C 30.3, H 3.35, N 19.3. ^{1}H NMR (300 MHz, ^2H_2O): δ = 9.03 (s, 1 H, H$^{2'}$), 8.93 (m, 1 H, H^2), 8.13 (m, 1 H, H^3), 3.06 (m, 2 H, H^5), 2.90 (m, 2 H, H^6), 3.33 (s, 1 H, SH) ppm. For comparison purposes: PZT: ^{1}H NMR (300 MHz, ^2H_2O): δ = 8.41 (m, 2 H, H^2 and H$^{2'}$), 8.35 (m, 1 H, H^3), 2.99 (t, J = 6.9 Hz, 2 H, H^5), (t, J = 6.9 Hz, 2 H, H^6), 1.43 (shoulder, SH) ppm. PZT: ^{1}H NMR (300 MHz, C^2HCl_3): δ = 8.535 (m, J' = 2.7 Hz, J'' = 1.5 Hz, 1 H, H^2), (d, J = 1.5 Hz, 1 H, H$^{2'}$), (d, J = 2.7 Hz, 1 H, H^3), 3.132 (t, J = 6.9 Hz, 2 H, H^5), 2.978 (m, J' = 6.9 Hz, J'' = 1 Hz, 2 H, H^6), 1.46 (t, J = 8.2 Hz, 1 H, SH) ppm. CV for $Na_3[Fe(CN)_5PZT]{\cdot}3H_2O$: $E_{1/2}$ = +0.55 V (SCE). For comparison purposes: $[Fe(CN)_5pz]^{3-}$ (where pz = pyrazine): $E_{1/2}$ = +0.55 V (SCE).[8]

Physical Measurements: NMR spectra were recorded with a Varian 300 MHz (INOVA 1) spectrometer using 1×10^{-2} mol dm^{-3} solutions. All peaks were related to tetramethylsilane (TMS). Cyclic and differential pulse voltammetry measurements were carried out with an Autolab PGSTAT 30 potentiostat/galvanostat with a conventional three-electrode cell constituted by a carbon glass disk working electrode (0.196 cm^2), a coiled platinum wire as the counter electrode, and an Ag/AgCl (KCl 0.1 mol dm^{-3}) reference electrode. The electrolyte employed was 0.1 mol dm^{-3} KCl in water containing 1 mmol dm^{-3} of the iron complex. UV/Vis spectra and kinetics experiments were recorded with a Hewlett Packard model HP-8453 diode-array spectrophotometer with a thermostatted cell holder. FT-IR spectra were recorded with a Shimadzu model FTIR 8300 spectrophotometer. Raman measurements were performed using an InPhotote portable instrument equipped with Raman probe optical fiber and a 300-mW (785 nm) diode laser (resolution of 6 cm^{-1} and 350–2000 cm^{-1} spectral range). Typically, an accumulation time of 120 s was employed to obtain the Raman spectra. For the free PZT and $Na_3[Fe(CN)_5PZT]{\cdot}3H_2O$ complex, the Raman spectra were recorded from pure sample and 1 mol dm^{-3} aqueous solution, respectively. SERS measurements were performed using 1×10^{-5} mol dm^{-3} aqueous solutions. The dissoci-

ation kinetics of $[Fe(CN)_5PZT]^{3-}$ were studied in the presence of a large excess of dimethyl sulfoxide (dmso), at 25.0 ± 0.1 °C and 0.1 mol dm^{-3} LiCl. The disappearance of the MLCT band of the $[Fe(CN)_5PZT]^{3-}$ species at 461 nm, was monitored under pseudo-first-order conditions, and the observed rate constants, k_{obs}, were obtained by linear fitting of $\ln(A_\infty/A_t)$ vs. time. For the evaluation of the dissociation kinetic constants of the gold nanoparticles stabilized with the iron complex, the changes of optical density at 460 nm were plotted vs. time, yielding a single exponential curve. The kinetic constant was obtained by a simplex fitting of this curve, according to the equation $y = y_0 + A\exp(-kt)$.

Theoretical Calculations: The DFT method was employed for geometry optimization, using GAMESS[36] software running on a PC cluster. Becke's three-parameter hybrid functional[37] with the LYP correlation functional[38] (B3LYP) was employed with a 6-31G(d,p) basis set for all atoms. Semi-empirical calculations were performed using the HYPERCHEM software package.[39] Theoretical calculations of the electronic spectrum were carried out using ZINDO/S,[40] employing a convergence criterion of 10^{-7} kcal mol^{-1} for SCF and single CI excitations, using an active space of 40 frontier molecular orbitals (20 highest occupied and 20 lowest unoccupied MOs). The harmonic vibrational frequencies and intensities were calculated at this same level of theory, based on the analytical evaluation of second derivatives of energy as a function of atomic coordinates. Raman intensities were simulated by the numerical differentiation procedure of Komornicki and others,[41,42] applying an intensity of 2×10^{-3} a.u. for the electric field.

Acknowledgments

The authors gratefully acknowledge the financial support from Fundacao de Amparo a Pesquisa do Estado de Sao Paulo (FAPESP), Conselho Nacional de Desinvolvimento Cientifico e Tecnologico (CNPq), and Instituto do Milenio de Materiais Complexos (IM2C). S. H. T. thanks the Centro Brasileiro-Argentino de Nanotecnologia and Professors D. Zanchet, E. J. Calvo, M. Brust, and D. J. Schiffrin, for their precious lectures at the "Escuela de Nanopartículas" in Buenos Ayres.

[1] M. C. Daniel, D. Astruc, *Chem. Rev.* **2004**, *104*, 293–346.
[2] Y. Yang, S. Matsubara, M. Nogami, J. Shi, W. Huang, *Nanotechnology* **2006**, *17*, 2821–2827.
[3] E. Katz, I. Willner, *Angew. Chem. Int. Ed.* **2004**, *43*, 6042–6108.
[4] K. G. Thomas, P. V. Kamat, *Acc. Chem. Res.* **2003**, *36*, 888–898.
[5] A. J. Viudez, R. Madueno, T. Pineda, M. Blazquez, *J. Phys. Chem. B* **2006**, *110*, 17840–17847.
[6] H.-L. Zhang, D. S. Evans, J. R. Henderson, R. E. Miles, T. Shen, *J. Phys. Chem. B* **2003**, *107*, 6087–6095.
[7] F. S. Nunes, L. S. Bonifacio, K. Araki, H. E. Toma, *Inorg. Chem.* **2006**, *45*, 94–101.
[8] H. E. Toma, J. M. Malin, *Inorg. Chem.* **1973**, *12*, 1039–1045.
[9] H. E. Toma, J. M. Malin, *Inorg. Chem.* **1973**, *12*, 2080–2084.
[10] H. E. Toma, J. M. Malin, E. Giesbrecht, *Inorg. Chem.* **1973**, *12*, 2084–2089.
[11] H. E. Toma, J. M. Martins, E. Giesbrecht, *J. Chem. Soc. Dalton Trans.* **1978**, 1610–1617.
[12] H. E. Toma, A. A. Batista, H. B. Gray, *J. Am. Chem. Soc.* **1982**, *104*, 7509–7515.
[13] H. E. Toma, A. L. Coelho, H. M. Malin, *Inorg. Chem.* **1983**, *22*, 2703–2707.
[14] H. E. Toma, M. S. Takasugi, *Polyhedron* **1982**, *1*, 429–436.
[15] S. S. S. Borges, A. L. Coelho, I. S. Moreira, M. A. B. Araújo, *Polyhedron* **1994**, *13*, 1015–1022.
[16] L. M. Baraldo, P. F. Forlano, A. R. Parise, L. D. Slep, J. A. Olabe, *Coord. Chem. Rev.* **2001**, *219*, 881–921.
[17] J. M. Malin, C. F. Schmidt, H. E. Toma, *Inorg. Chem.* **1975**, *14*, 2924–2928.
[18] J. Burges, *Spectrochim. Acta, Part A* **1970**, *26*, 1369–1374.
[19] J. Burges, *Spectrochim. Acta, Part A* **1970**, *26*, 1957–1962.
[20] H. E. Toma, M. S. Takasugi, *J. Solution Chem.* **1983**, *12*, 547–561.
[21] H. E. Toma, M. S. Takasugi, *Polyhedron* **1989**, *8*, 941–945.
[22] H. E. Toma, M. S. Takasugi, *J. Solution Chem.* **1989**, *18*, 575–583.
[23] U. Mayer, *Pure Appl. Chem.* **1979**, *51*, 1697–1712.
[24] G. Mie, *Ann. Phys.* **1908**, *25*, 377.
[25] M. Moskovits, *Rev. Mod. Phys.* **1985**, *57*, 783–826.
[26] A. Otto, I. Mrozek, H. Grabhorn, W. Akemann, *J. Phys.: Condens. Matter* **1992**, *4*, 1143–1212.
[27] R. Aroca, *Surface-Enhanced Vibrational Spectroscopy*, John Wiley & Sons, Chichester, England, **2006**.
[28] J. C. Rubim, P. Corio, M. C. C. Ribeiro, M. Matz, *J. Phys. Chem.* **1995**, *99*, 15765–15774.
[29] H. E. Toma, *J. Chem. Soc. Dalton Trans.* **1980**, 471–475.
[30] H. E. Toma, *Can. J. Chem.* **1979**, *57*, 2079–2084.
[31] K. Szacilowski, W. Macyk, M. Hebda, G. Stochel, *Chemphyschem* **2006**, *7*, 2384–2391.
[32] K. G. Thomas, P. V. Kamat, *Acc. Chem. Res.* **2003**, *36*, 888–898.
[33] H. E. Toma, C. Creutz, *Inorg. Chem.* **1977**, *76*, 545–550.
[34] G. Brauer, *Handbook of Preparative Inorganic Chemistry*, 2nd ed., Academic Press, New York, **1965**, vol. 2, p. 1511.
[35] J. Turkevitch, P. C. Stevenson, J. Hilier, *Discuss. Faraday Soc.* **1951**, *11*, 55.
[36] M. W. Schmidt, K. K. Baldridge, J. A. Boatz, S. T. Elbert, M. S. Gordon, J. J. Jensen, S. Koseki, N. Matsunaga, K. A. Nguyen, S. Su, T. L. Windus, M. Dupuis, J. A. Montgomery, *J. Comput. Chem.* **1993**, *14*, 1347–1363.
[37] A. D. Becke, *J. Chem. Phys.* **1993**, *98*, 5648.
[38] C. Lee, W. Yang, R. G. Parr, *Phys. Rev. B* **1988**, *37*, 785.
[39] Hypercube Inc., Gainesville, FL, USA, **2002**.
[40] a) M. C. Zerner, G. H. Loew, R. F. Kirchner, U. T. Mueller-Westerhoff, *J. Am. Chem. Soc.* **1980**, *102*, 589; b) J. E. Ridley, M. C. Zerner, *Theor. Chim. Acta* **1976**, *42*, 223; c) J. E. Ridley, M. C. Zerner, *Theor. Chim. Acta* **1973**, *32*, 111; d) A. D. Bacon, M. C. Zerner, *Theor. Chim. Acta* **1979**, *53*, 21.
[41] A. Komornicki, J. W. McIver, *J. Chem. Phys.* **1979**, *70*, 2014.
[42] G. B. Bacskay, S. Saebo, P. R. Taylor, *Chem. Phys.* **1984**, *90*, 215.

Received: February 1, 2007
Published Online: June 14, 2007

